Dzyaloshinskii-Moriya interaction in symmetric epitaxial $[Co/Pd(111)]_N$ superlattices with different numbers of Co/Pd bilayers

A. V. Davydenko,[1,*] A. G. Kozlov,[1] A. G. Kolesnikov,[1] M. E. Stebliy,[1] G. S. Suslin,[1]
Yu. E. Vekovshinin,[1] A. V. Sadovnikov,[2] and S. A. Nikitov[2]

[1]*Laboratory of Thin Film Technologies, School of Natural Sciences, Far Eastern Federal University, Vladivostok 690950, Russian Federation*
[2]*Laboratory "Metamaterials," Saratov State University, Saratov 410012, Russian Federation*
and Kotel'nikov Institute of Radioengineering and Electronics, Russian Academy of Sciences, Moscow, Russian Federation

(Received 25 October 2018; revised manuscript received 25 December 2018; published 25 January 2019)

Heavy metal/ferromagnetic superlattices are of great interest since Néel skyrmions may be stabilized in them due to an interfacial Dzyaloshinskii-Moriya interaction even at room temperature. Here we report on evidence of the strong Dzyaloshinskii-Moriya interaction in symmetric epitaxial $[Co/Pd(111)]_N$ superlattices with high perpendicular magnetic anisotropy. The structural and magnetic properties of epitaxial $[Co/Pd(111)]_N$ superlattices were investigated dependent on the number of Co/Pd bilayers. Based on comparison of the periodicity of experimentally obtained demagnetized patterns and simulated magnetic structures, a strong increase of the effective Dzyaloshinskii-Moriya interaction constant with increase of the period N of $[Co/Pd(111)]_N$ superlattices is established. The origin of Dzyaloshinskii-Moriya interaction and its behavior in the symmetric $[Co/Pd(111)]_N$ system is discussed.

DOI: 10.1103/PhysRevB.99.014433

I. INTRODUCTION

Antisymmetric Dzyaloshinskii-Moriya interaction (DMI) in combination with symmetric exchange interaction and perpendicular magnetic anisotropy (PMA) leads to various magnetization structures in thin films like skyrmions [1,2], skyrmion lattices [3], spin spirals [4,5], and chiral Néel domain walls (DWs) [6,7]. DMI can be induced in the magnetic medium with strong spin-orbit coupling and a lack of inversion symmetry [8,9]. In magnetic ultrathin films and superlattices these conditions are fulfilled at the interfaces of ferromagnetic metal (FM) layers and heavy metal (HM) layers with large spin-orbit coupling [10]. Strong spin-orbit coupling at the HM/FM interfaces is believed to cause a family of spin-orbit effects apart from DMI: PMA [11], Rashba coupling [12], and the spin Hall effect [13]. It was observed that chiral Néel DWs and Neel skyrmions in ultrathin HM/FM systems could be very efficiently displaced under the action of in-plane current pulses due to the transferring of so-called spin-orbit torque (SOT), a generic effect including physical mechanisms of spin momentum transfer generated by Rashba or spin Hall effects [14]. Therefore, structures possessing high SOT efficiency and DMI are potential candidates for future racetrack memories based on skyrmions or chiral Néel DWs [15,16].

The opportunity of precise control of the energy of DMI in the racetrack medium is of high importance because DMI has a strong influence on the skyrmion sizes [1], structure of DWs [6], and SOT efficiency [17]. It is worth noting that the type of magnetic structure in the ultrathin magnetic film with DMI also strongly depends on the energies of the PMA and exchange interaction [3,18]. The energy of exchange interaction is difficult to control precisely. The most straightforward approach to controlling the energy of PMA is through variation of the thickness of the magnetic layers in the magnetic system [19], but in most cases DMI in ultrathin films is of interface origin and hence depends on the thickness of the magnetic layer in the same manner as PMA [20].

Methods of controlling the energy of DMI in ultrathin films are reduced to the following: choosing different materials for HM layers with opposite signed DMI of the bottom and top interfaces in HM1/FM/HM2 systems [1,3], modification of the interfaces by deposition of submonolayer coverages of different materials [21], oxidation of the interfaces [22], and modification of the interface properties—sharpness, roughness, and strains [23].

In the most recent papers concerning DMI, special attention is paid to the investigation of superlattices—systems in which the HM1/FM/HM2 structure repeats N times [1,3,24]. An advantage of superlattices over trilayered systems is related to their high thermal stability and magnetic signal. Moreover, dipolar interaction demagnetizes superlattices with large effective thicknesses and stabilizes skyrmions in them, even if the energy of the effective DMI in superlattices is quite low. It is reasonable to consider that the effective DMI in superlattices is nearly the same as in the structures consisting of one period, because increasing the number of interfaces is compensated by increasing the total magnetic volume. However, Pollard *et al.* found an increase of the energy of the effective DMI with increase of the number of Co/Pd bilayers in the $Pt/[Co/Pd]_N$ polycrystalline system [25]. The approach of controlling the energy of DMI by choosing an appropriate value of the period of superlattices seems to be promising since the energies of PMA and exchange interaction may not depend on the period of the superlattices. In this work we

*avdavydenko@gmail.com

investigated epitaxial $[Co/Pd(111)]_N$ superlattices and found behavior of the effective DMI constant similar to that reported in the paper by Pollard *et al.*, but the estimated values of the energies of DMI in epitaxial superlattices are larger than in polycrystalline ones.

II. EXPERIMENT

The samples were grown in an ultrahigh-vacuum complex Omicron, which consisted of a preparation molecular beam epitaxy chamber and an analysis chamber interconnected with each other. We used Si(111) substrates misoriented towards [11-2] by 0.1°. Before loading into the chamber, the Si(111) substrates were rinsed in isopropyl and distilled water. Then the substrates were heated at 500 °C by indirect heating for 12 h. Just before deposition, samples were flash heated by direct current at 1200 °C three times for 10 s and slowly cooled down to room temperature. All the metals were evaporated from high-temperature effusion cells. The rates of growth of Cu, Co, and Pd were 0.9, 0.22, and 0.2 nm/min, respectively. The rates of deposition were monitored by a quartz crystal microbalance. Calibration of the quartz crystal microbalance was performed by means of reflection high-energy electron diffraction (RHEED). We detected the oscillations of the intensity of the specular beam reflection during the growth of Cu on Si(111), Co on Si(111)/Cu(1 nm), and Pd on Si(111)/Cu(1 nm). Then we calculated the period of the oscillations and compared it with data obtained from the quartz crystal microbalance. The temperature of the substrates was varied from 75 °C during Cu buffer layer deposition to 120 °C during deposition of the top Co and Pd layers in the thickest samples. Changes in the temperature of the samples during the deposition of different materials were caused by different radiative heating of the samples from the effusion cells. Epitaxial $[Co(0.8\,nm)/Pd(2\,nm)]_N$ superlattices were grown on a Si(111)/Cu(2 nm)/Pd(3 nm) surface. A Cu(2 nm) buffer layer was formed on a Si(111) substrate to prevent intermixing of Pd and Si and to initiate epitaxial growth of fcc Pd(111). The thickness of the cap Pd layer was 3 nm, which is sufficient to prevent oxidization of the structure. The investigated periods of the superlattices were 1, 2, 3, 4, 5, 10, and 20. In the following text, a superlattice with a given period N, for example, equal to 5, will be simply denoted as $N5$.

Growth processes and roughness were investigated *in situ* using a scanning tunneling microscope (STM) manufactured by Omicron. STM images were obtained on the same sample by alternation of the deposition and scanning processes. The lattice period of the metal layers during growth and their structure were analyzed by means of reflection high-energy electron diffraction (RHEED) (Staib Instruments). RHEED measurements were done simultaneously with deposition of the samples. Magnetic characterization of the samples was carried out using a vibrating sample magnetometer (VSM) with magnetic fields up to 27 kOe, manufactured by Lakeshore. Magnetic structure was measured by a magneto-optical Kerr effect (MOKE) microscope (Evico-magnetics) and magnetic-force microscope (NT-MDT). The MOKE microscope was equipped with a handmade coil applying out-of-plane magnetic fields and an in-plane electromagnet. Magnetic force microscopy (MFM) images were obtained in the switched-off feedback loop mode using MFM-HM tips manufactured by NT-MDT. The typical distance between the sample surface and magnetic tip was 50 nm. Micromagnetic simulations were carried out using MUMAX3 software [26]. To simulate the equilibrium domain structure of the multilayered films we used a single-layer effective model comprehensively described in [3]. In this model, the multilayers can be effectively treated as a single-layer film with effective thickness $d_{\text{eff}} = N \times (d_{\text{Co}} + d_{\text{Pd}})$, where N is the period of the superlattice; $d_{\text{Co}} = 0.8$ nm and $d_{\text{Pd}} = 2$ nm are the thicknesses of the Co and Pd layers, respectively. Magnetic constants are scaled by a factor $f = d_{\text{Co}}/(d_{\text{Co}} + d_{\text{Pd}}) = 0.286$. We also tested a precise model with a thorough simulation of all the layers of superlattices, but we did not find any significant differences in the results. The size of the simulation area was 2000 nm × 2000 nm × (N2.8) nm. The cell size was 2 nm × 2 nm × (N2.8) nm. Two-dimensional (2D) periodic boundary conditions were used in the modeling. The total energy of the system was minimized by the steepest conjugate gradient method with the built-in function MINIMIZE(). The RELAX() function was used in the case of $N5$ superlattices with a rectangular hysteresis loop in which the MINIMIZE() algorithm does not converge well. The stopping criterion MINIMIZERSTOP for energy minimization was set to 5×10^{-5}. The saturation magnetization and energies of PMA were determined from the experiment. The considered values of the exchange constants were 20, 25, and 30 pJ/m.

III. RESULTS AND DISCUSSION

A. Growth processes and structure of the layers

A Cu(2 nm) buffer layer was formed on the Si(111) substrate to prevent intermixing of Pd and Si and to initiate epitaxial growth of fcc Pd(111). Cu(111) grows on Si(111) in a layer-by-layer 2D growth mode starting from the thickness of 0.6 nm. The epitaxial relationships defined from the RHEED patterns are Cu(111)||Si(111) and $Cu_{[11\text{-}2]}||Si_{[10\text{-}1]}$. The epitaxial relationships during growth of the subsequent Pd and Co layers remain the same as in Cu. Pd(111) grows on Cu(111) and Co(111) surfaces in fcc structure. The RHEED streaks from the Pd surface of each layer are sharp, which indicates relaxed and relatively smooth surfaces [Fig. 1(a)]. It is not possible to clearly define whether Co grows by fcc or hcp structure only from the RHEED patterns [27]. However, the absence of strong magnetocrystalline anisotropy in the [Co/Pd(111)] superlattices in the direction perpendicular to the plane of the films indicated that Co grows predominantly in fcc structure. The RHEED streaks from the surface of the Co layers are more diffuse and obscure compared to the RHEED streaks from the Pd surface [Fig. 1(b)]. This may be explained by the large amount of misfit dislocations and stacking faults in the Co layers [28]. The evolution of the lattice parameter of the Co layers during the growth of the superlattices was measured by RHEED [Fig. 1(c)]. The large 9.6% lattice mismatch between the Co and Pd leads to the misfit dislocations formation from the beginning of the growth of the Co layers. Hence, the Co lattice parameter gradually decreases with increase of the Co coverage. The profiles of relaxation

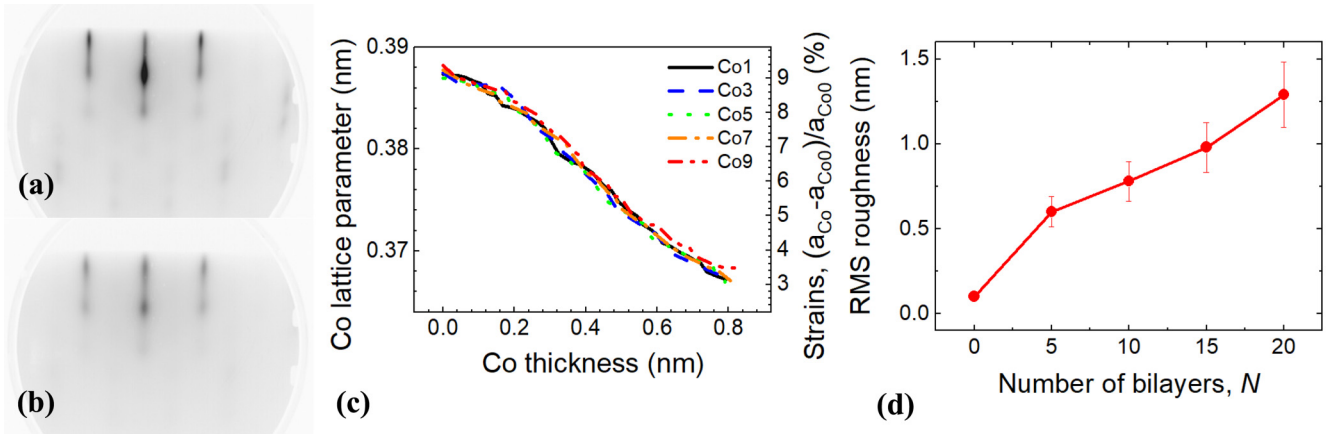

FIG. 1. RHEED patterns of fifth (a) Pd and (b) Co layers in the $N10$ superlattice. (c) Co lattice parameter and strains in different Co layers of $N10$ sample. (d) Root-mean-square roughness of Pd layers during growth of $N20$ superlattice.

of different Co layers in the $[Co/Pd(111)]_N$ superlattices are similar. Hence, the Co layers are equally strained, independently of the number of Co layers. The bottom interfaces of the Co layers are more greatly strained (9.2%) as compared to the top Co interfaces (3.3%).

The roughness of the bottom Pd/Co interfaces was analyzed by STM during growth of the thickest $N20$ superlattice [Fig. 1(d)]. The roughness increases with increase of the number of bilayers. This behavior may be explained by the increasing roughness of epitaxial Pd films during their growth in (111) crystallographic orientation [29]. The roughness of the top Co/Pd interface of the chosen Co layer remains nearly the same as the roughness of the bottom Pd/Co interface. The Co layers even tend to smooth the rough surface caused by the growth of Pd layers [30].

B. Magnetometry measurements

Out-of-plane magnetic hysteresis loops of the $[Co/Pd]_N$ superlattices with different numbers of bilayers are shown in Fig. 2(a). With increase of the number of bilayers, the magnetostatic energy of the system increases, which results in demagnetization of the sample in the absence of magnetic fields. Hence, the magnetic structure of thicker superlattices in the remanence is the multidomain labyrinth state with near-zero-sum magnetic moment. The out-of-plane hysteresis loops of superlattices with large N become sheared relative to the M/M_s axis. This behavior is well explained by the model of periodic stripe domains in an infinite plate with uniaxial PMA, proposed by Kittel [31] and developed by Kooy and Enz [32]. The domains form because of a balance between the DW energy and the demagnetizing energy. Such hysteresis loops were observed in the Co/Pd and Co/Pt polycrystalline superlattices with increase of the number of bilayers [33]. However, in the multilayered structures with DMI, the demagnetizing effect may be much larger than when the demagnetization is only due to magnetostatic interaction.

The in-plane magnetic hysteresis loops of the $[Co/Pd]_N$ superlattices with different numbers of bilayers are outlined in Fig. 2(b). One can see that strong PMA persists in all samples. To calculate the energy of the PMA, the value of the saturation magnetization needs to be evaluated. The dependence of the magnetic moment normalized to the unity of an area on the number of bilayers N was measured in the $[Co/Pd]_N$ multilayers [Fig. 2(c)]. Linear dependence of the magnetic moment on the number of Co/Pd bilayers indicates that the saturation magnetization does not depend on the roughness of the interfaces, at least in the limit of the accuracy of the VSM measurements. The value of the magnetic moment normalized to the unity of an area of one Co/Pd period evaluated by the slope of the $m(N)$ curve is 1.26×10^{-3} A. Using the value of the saturation magnetization of Pd, $M_{s,\mathrm{Pd}} = 3.1 \times 10^5$ A/m [34], and the bulk value of the saturation magnetization of Co, $M_{s,\mathrm{Co}} = 1.42 \times 10^6$ A/m, the sum thickness of two polarized Pd layers in the bottom and in the top of each Co layer was determined to be $t_{\mathrm{Pd\,pol}} = 0.4$ nm. If one neglects Pd polarized layers with low magnetization and assumes that all the magnetic material is concentrated in the Co layer of 0.8 nm thickness, then the value of the saturation magnetization is 1.58×10^6 A/m. This value of magnetization was used in the calculation of the energy of PMA.

The energy of the effective PMA calculated by an area method as a function of the period of superlattices is shown in Fig. 2(d). It appears that the effective energy of the PMA is independent of the number of bilayers N and fluctuates near the average value of $(8 \pm 1) \times 10^5$ J/m^3. This is reasonable because PMA depends on the strains in the Co layers and the structure of the interfaces, which remain the same in all the layers. In our previous work, it has been shown that the roughness of the bottom Pd/Co interface does not influence the energy of the PMA [30]. The results of the present paper corroborate this conclusion since the energy of PMA remains nearly the same despite continuously increasing the roughness of the interfaces in the upper layers.

C. DMI measurements

1. N1–N4 series

Measurements of the effective DMI field in superlattices with $N = 1$ and 2 were performed by an approach proposed by Je *et al.* [35]. DMI transforms Bloch DWs to Néel DWs with fixed chirality in the films with PMA. The growth of the circular bubble domain in the presence of in-plane and out-of-plane magnetic fields and DMI is asymmetrical. The DW

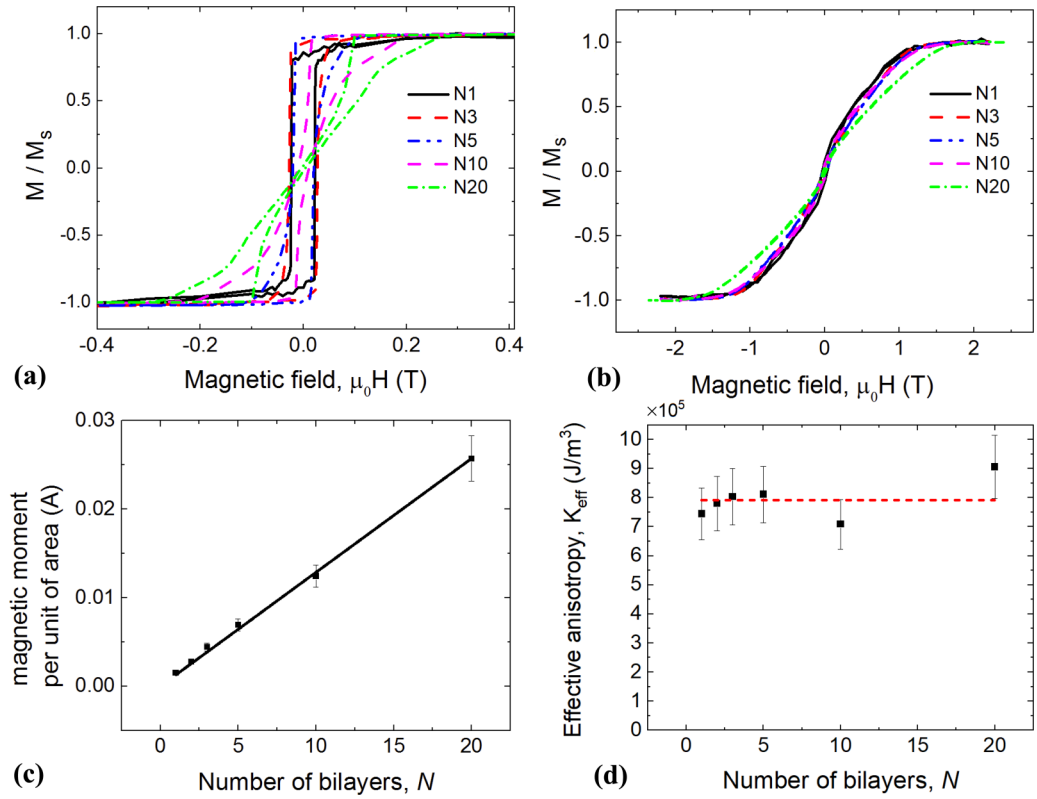

FIG. 2. (a) Out-of-plane and (b) in-plane hysteresis loops of crystalline $[Co/Pd]_N$ superlattices. The dependencies of (c) magnetic moment per unit of area and (d) energy of effective PMA on the period N in the $[Co/Pd]_N$ superlattices.

in which magnetic moments are curled in the direction of the applied in-plane magnetic field is propagating faster than the diametrically opposite DW, in which the magnetic moments are curled opposite to the in-plane magnetic field. The velocity of the oppositely curled DW decreases with increase of the in-plane magnetic field up to a certain minimal value at a critical magnetic field and increases in the magnetic fields that are larger than critical. This critical field is considered as the effective DMI field. The effective DMI energy may be derived from the effective DMI field using the expression [36]

$$D_{\text{eff}} = \mu_0 H_{\text{DMI}} M_s \Delta_0, \tag{1}$$

where $\Delta_0 = \sqrt{\frac{A}{K_{\text{eff}}}}$ is a DW width.

The method of measurement was as follows. First, the area of the sample with a stable nucleating domain was found. Prior to measuring the velocity curves careful alignment of the magnets relative to the sample plane was performed in the MOKE microscope. To eliminate the z component from the in-plane field, a maximal in-plane magnetic field of $\mu_0 H_x = 0.25$ T was applied in positive and negative directions. If the DWs began to move, the tilt of the magnets was compensated. More careful adjustment of the magnets was performed by comparison of the velocities of left and right DWs measured in negative and positive in-plane magnetic fields, respectively, under the simultaneous action of a constant out-of-plane magnetic field. If the velocities were different, the procedure of alignment was repeated. After the alignment procedure, videos of expansions of the domains were recorded using a CCD camera in the constant out-of-plane fields of -15 mT for $N1$ and -12 mT for $N2$ samples and different in-plane magnetic fields. The velocities of DW propagation were calculated by choosing several frames and measuring the distance by which the DW was displaced, divided by the time interval between the frames. The time interval between adjacent frames was 36 ms.

Asymmetrical domains grown in $N1$ and $N2$ superlattices in combination of in-plane and out-of-plane magnetic fields are shown in Figs. 3(a) and 3(c), respectively. In both cases domains contain a net of 360° Néel DWs, which is the sign of strong DMI in this system [37]. Net DMI from the bottom Pd/Co and top Co/Pd interfaces induces right-handed chirality in the Néel DWs; hence the sign of effective DMI in this system is negative [10,36]. The velocity curves of the left DWs in $N1$ and $N2$ samples are shown in Figs. 3(b) and 3(d), respectively. The effective DMI fields are equal to $\mu_0 H_{\text{DMI}} = -102 \pm 7$ and -130 ± 10 mT in $N1$ and $N2$ superlattices, respectively. The calculated effective DMI energies in the $N1$ sample for exchange constants 20, 25, and 30 pJ/m are -0.83 ± 0.06, -0.93 ± 0.06, and -1.02 ± 0.07 mJ/m^2, respectively. The calculated effective DMI energies in the $N2$ sample for exchange constants 20, 25, and 30 pJ/m are -1.03 ± 0.08, -1.15 ± 0.09, and -1.26 ± 0.1 mJ/m^2, respectively. All the given and derived magnetic parameters of $[Co/Pd]_N$ superlattices are outlined in Table I for clarity.

Velocity measurements in superlattices with N larger than 2 become difficult because multiple domains are nucleated and merge with each other during growth; the shape of the DWs becomes wavy. We have not been able to reach minimum in the velocity curves of the left DWs in the $N3$ and $N4$

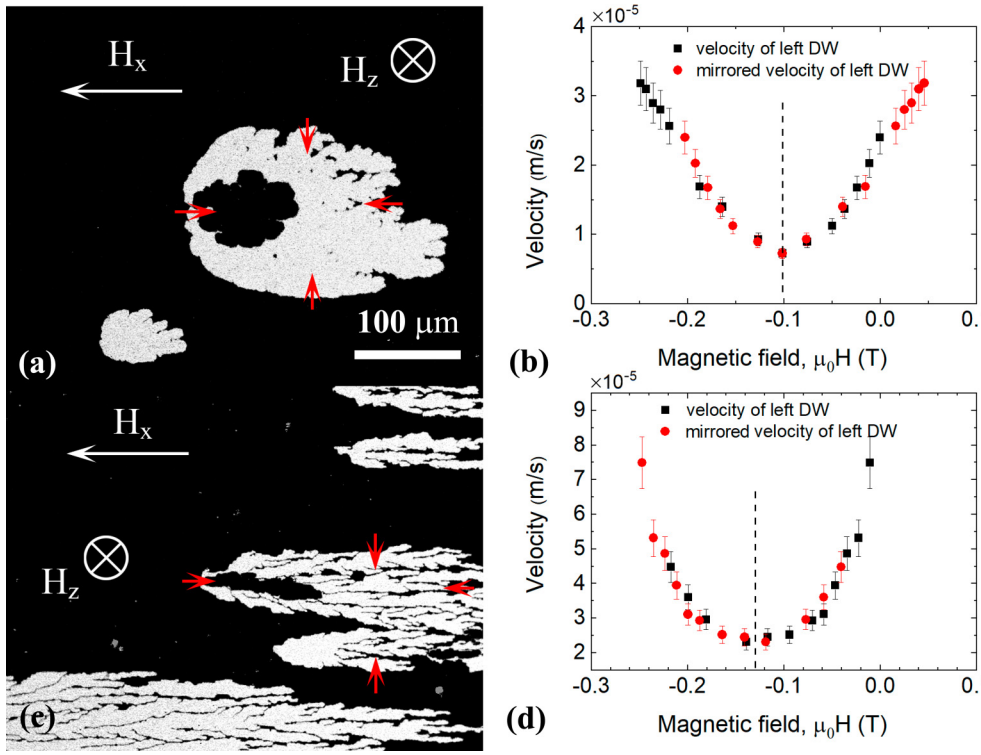

FIG. 3. (a), (c) Asymmetrically growing domain in combination of in-plane and out-of-plane magnetic fields in $N1$ and $N2$ samples, respectively. Black area in the middle of the domain is obtained due to subtraction of the initial domain area. (b,d) Dependencies of the velocities of the left DWs on the magnitude of the in-plane field in $N1$ and $N2$ samples, respectively. Red dots denote the same experimental points but mirrored from the axis of symmetry at $H = H_{\mathrm{DMI}}$ and hence inserted in the positions $(2H_{\mathrm{DMI}} - H_x)$. Red arrows denote the direction of the magnetization in Néel DWs.

samples because in high negative in-plane magnetic fields velocities of the right walls become very large and spontaneously nucleated domains spread over the whole observable area. However, the measurements reveal that the magnitude of the effective DMI in $N3$ and $N4$ samples at least does not decrease as compared with N2 superlattices and right-handed chirality in the Néel DWs is conserved.

2. N10–N20 series

It was shown that the energy of effective DMI may be evaluated by comparing the periods of the experimentally obtained and simulated demagnetized stripe domain structures [3]. The samples with large PMA may be demagnetized close to the ground state only if the energy of DMI is quite large or if they self-demagnetize due to large magnetostatic energy. The latter takes place in the thick $[\mathrm{HM1/FM/(HM2)}]_N$ multilayered films with large interface PMA. Such samples are characterized by a sheared out-of-plane hysteresis loop and the M_r/M_s ratio less than 1.

Equilibrium domain structures were experimentally obtained by demagnetization of the samples in decaying alternating magnetic fields oriented in and out of the plane of the films. The domain structures of $N10$ and $N20$ superlattices demagnetized by in-plane oriented magnetic field are shown in Figs. 4(a) and 4(c), respectively. The labyrinth domain structure is regular and predominantly oriented along the direction of the applied in-plane demagnetizing magnetic field in the $N20$ sample. In the $N10$ superlattice, domain structure is irregular and more isotropic. The periodicity of the magnetic

TABLE I. Parameters of the epitaxial $[\mathrm{Co/Pd(111)}]_N$ superlattices.

					D_{eff} (mJ/m^2)		
					A (pJ/m)		
N	M_s (kA/m)	K_{eff} (MJ/m)	$\lambda_{\mathrm{ip\ expt}}$ (nm)	$\lambda_{\mathrm{op\ expt}}$ (nm)	20	25	30
1		0.74			−0.83 ± 0.06	−0.93 ± 0.06	−1.02 ± 0.07
2		0.8			−1.03 ± 0.08	−1.15 ± 0.09	−1.26 ± 0.1
5	1580	0.81	600 ± 80	780 ± 100	−1.6 ± 0.35	−2.2 ± 0.5	−2.7 ± 0.6
10		0.71	330 ± 40	410 ± 30	−1.85 ± 0.45	−2.55 ± 0.4	−3.2 ± 0.46
20		0.91	260 ± 20	315 ± 20	−2.3 ± 0.5	−3.22 ± 0.58	−4 ± 0.53

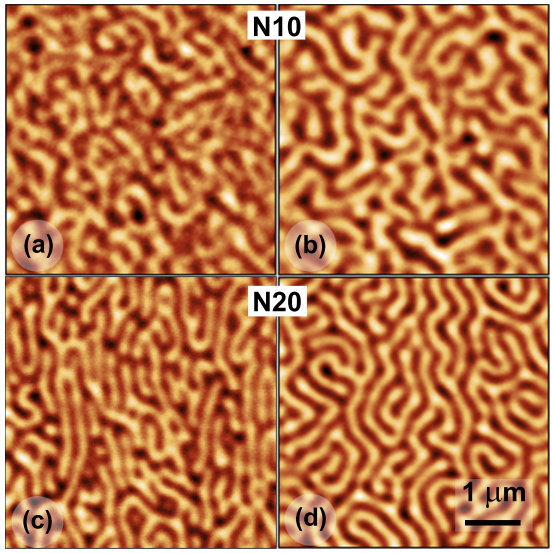

FIG. 4. MFM images of (a), (c) in-plane and (b), (d) out-of-plane demagnetized domain structures of $N10$ and $N20$ superlattices, respectively.

structures was determined by statistical analysis of the 20–30 random profiles between adjacent domains. The experimentally measured periods of the domain structures for $N10$ and $N20$ superlattices demagnetized by in-plane magnetic fields, λ_{ip}, are 330 ± 40, and 260 ± 20 nm, respectively.

The demagnetized structures of $N10$ and $N20$ superlattices obtained by out-of-plane alternate fields are shown in Figs. 4(b) and 4(d), respectively. The domain structures are isotropic in both superlattices, since the out-of-plane field does not prefer any anisotropy of domains. The periods of the structures are 1.2−1.25 times higher than the periods of the domain structures obtained by in-plane magnetic fields. The values of the periods of the domains for the $N10$ and $N20$ superlattices demagnetized in the out-of-plane magnetic fields, λ_{op}, are 410 ± 30, and 315 ± 20 nm, respectively. The period of the stripe domain structure decreases with increase of the effective thickness of the superlattices. Similar behavior of polycrystalline $[Co/Pt]_N$ multilayers was observed in [33] and it is in qualitative accordance with the classical model of Kooy and Enz in the limit of ultrathin films [32].

Thorough simulation of the demagnetization procedure by alternate magnetic fields is time consuming; hence, usually the demagnetized state is obtained by the relaxation of the initial random state in micromagnetic simulations [3,24]. Relaxation from a random state in zero magnetic field leads to the presence of a large number of skyrmions in relaxed states which does not coincide with the experimental images. In the present paper, the stripe domain structures of the $N10$ and $N20$ superlattices were obtained by relaxation from the initially saturated state with two skyrmions, which served as nucleation sites, in the absence of magnetic fields. The diameter of the skyrmions was 100 nm. In this case, periodic stripe domain structures develop by growing of the stripes from the skyrmions and look more like the experimentally obtained ones. The values of the periods of the domain structures relaxed from a random state are slightly lower than the periods of labyrinth phases relaxed from the saturated state with skyrmions. The periods of the simulated labyrinth structures were determined by averaging 20–30 periods between different domains.

The use of an appropriate value of exchange constant is needed for derivation of correct values of effective DMI energies from micromagnetic simulations. In many publications concerning sputtered Co films, the value of the exchange constant used in micromagnetic simulations is in the range of values 10−16 pJ/m [1,3,24]. The experimentally measured values of the exchange constant of crystalline Co are 25−28 pJ/m [38,39]. It was experimentally [40] and theoretically [41] shown that the exchange stiffness is independent of the Co fcc or hcp structure. Reduction of the exchange constant in polycrystalline Co may be explained by increased intermixing during the growth of sputtered films [42]. In the micromagnetic simulations, we used values of $A = 25$ pJ/m as basic and values of 20 and 30 pJ/m for comparison.

The dependencies of the periods of the simulated labyrinth structures on the DMI energy for $N10$ superlattices with different exchange constants are shown in Fig. 5(a). Intersection of the fitted curves of the simulated periods with the values of the periods obtained experimentally gives the values of the DMI constants. Micromagnetic modeling gives identical periods of the labyrinth structures with positive and negative effective DMI energies. Since there are no physical reasons for changing the sign of the effective DMI constant in $[Co/Pd]_N$ superlattices with increase of N larger than 4, we considered negative effective DMI energies for all investigated samples based on the results obtained from the $N1$-$N4$ superlattices. The derived effective DMI energies in the $N10$ sample for $A = 20$, 25, and 30 pJ/m are -1.85 ± 0.45, -2.55 ± 0.4, and -3.2 ± 0.46 mJ/m^2, respectively (see Table I) if one compares the simulated periods with the experimentally measured periodicity of in-plane demagnetized samples. Comparison of the periods of the simulated domain structures with the value of the period measured in out-of-plane demagnetized samples gives effective DMI energies of -1.3 ± 0.3, -2.1 ± 0.3, and -2.7 ± 0.27 mJ/m^2 for $A = 20, 25$, and 30 pJ/m, respectively. The hysteresis loops of $N10$ multilayer samples were simulated with $D_{\text{eff}} = -1.85$, -2.55, and -3.2 mJ/m^2 and $A = 20$, 25, and 30 pJ/m, respectively [Fig. 5(b)]. It appeared that the simulated hysteresis loops practically do not depend on the exchange energies, except for the area of high negative fields in which chiral Néel DWs are annihilated. Nevertheless, for both $N10$ and $N20$ superlattices a better coincidence of the simulated and experimental hysteresis loops is achieved when using the value of $A = 25$ pJ/m.

In Figs. 5(c)–5(h) simulated hysteresis loops are shown for the exchange constant 25 pJ/m and the values of effective DMI energies in the range of $-(1.55$–$4.05)$ mJ/m^2. As the criterion of coincidence, we analyzed tilting of the hysteresis loop in the near-zero magnetic fields in which reversible displacement of DWs occurs. The hysteresis loop simulated with $D = -2.55$ mJ/m^2 best coincides with the experimental loop. Based on the analysis of the simulated hysteresis loops, it may be concluded that superlattices must be demagnetized by in-plane magnetic fields to achieve the ground state and for comparison with simulated domain structures.

Dependencies of the periods of the simulated labyrinth structures on the DMI energy for $N20$ superlattices with

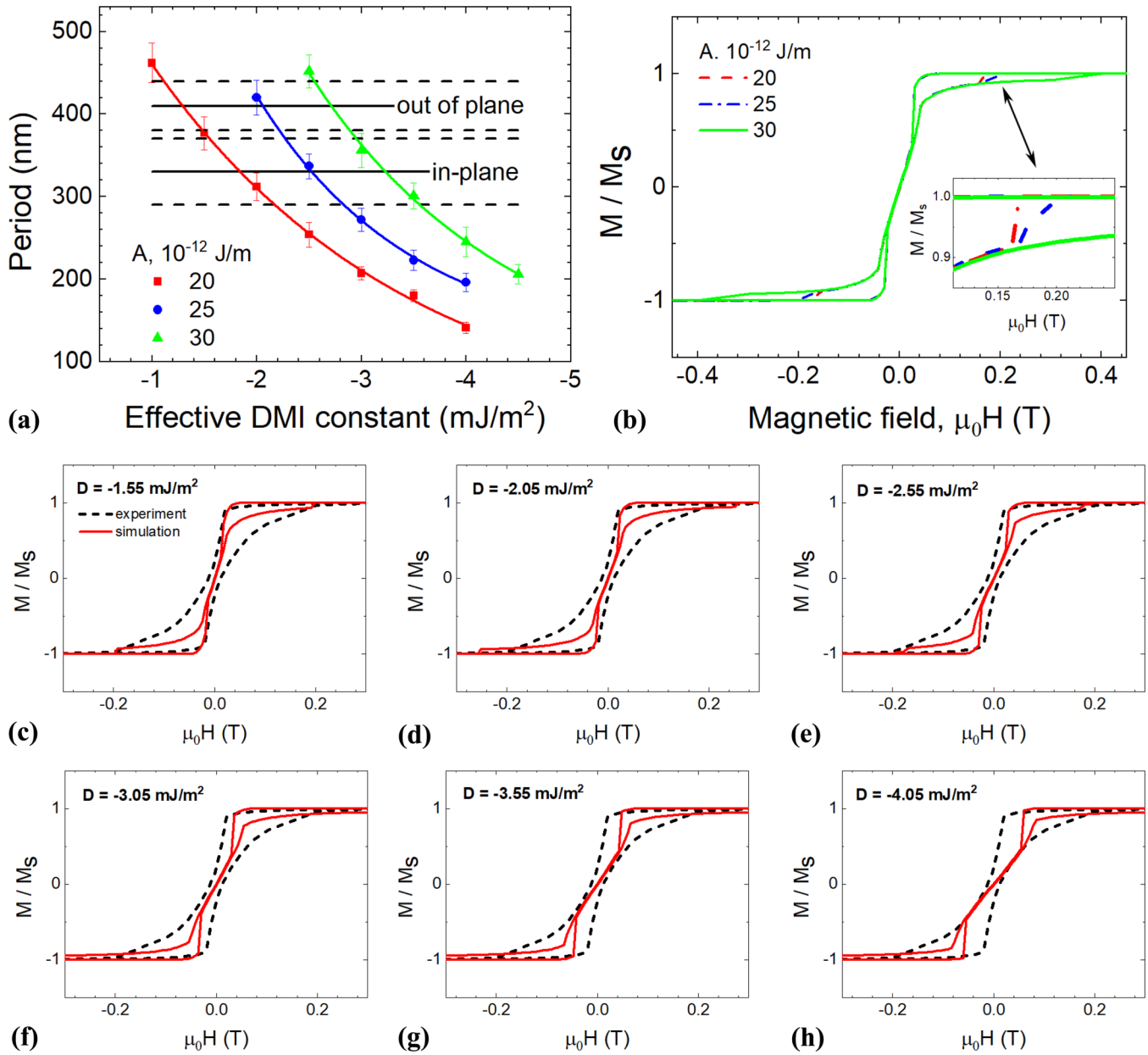

FIG. 5. (a) The dependencies of the periods of simulated magnetic structures of $N10$ superlattices on the energy of effective DMI. (b) Comparison of hysteresis loops of $N10$ samples simulated with parameters $A = 20$, 25, and 30 pJ/m and $D = -1.85$, -2.55, and $-3.2\,\mathrm{mJ/m^2}$, respectively. Hysteresis loops simulated for $N10$ structures with $A = 25\,\mathrm{pJ/m}$ and the values of effective DMI energy: (c) -1.55, (d) -2.05, (e) -2.55, (f) -3.05, (g) -3.55, and (h) $-4.05\,\mathrm{mJ/m^2}$.

different exchange constants are shown in Fig. 6(a). The derived effective DMI energies in the $N20$ sample for $A = 20$, 25, and 30 pJ/m are -2.3 ± 0.5, -3.22 ± 0.58, and $-4 \pm 0.53\,\mathrm{mJ/m^2}$, respectively (see Table I) if one compares the simulated periods with the experimentally measured periodicity of the in-plane demagnetized samples. The hysteresis loops of $N20$ multilayer samples simulated with DMI constants $D = -2.3$, -3.22, and $-4\,\mathrm{mJ/m^2}$ and $A = 20$, 25, and 30 pJ/m, respectively, are similar [Fig. 6(b)]. In Figs. 6(c)–6(h) simulated hysteresis loops are shown for $A = 25\,\mathrm{pJ/m}$ and the values of the effective DMI energies in the range of $-(2.22 - 4.72)\,\mathrm{mJ/m^2}$. In the case of $N20$ superlattices, the best coincidence of simulated and experimental hysteresis loops is achieved for the value $D_{\mathrm{eff}} = -3.72\,\mathrm{mJ/m^2}$, which is even larger by magnitude than the value $-3.22\,\mathrm{mJ/m^2}$ obtained by periodicity analysis and much larger than $-2.4\,\mathrm{mJ/m^2}$, the value obtained by comparing the periods of the simulated magnetic structures with periodicity of out-of-plane demagnetized samples.

The overall shape of the best simulated and experimental loops is similar, but they do not coincide ideally. This may be explained by several reasons. First, an experimental loop is averaged over the entire sample including the edges of the film, where the magnetic properties may differ slightly. Better compliance between the experimental and modeled hysteresis loops may be obtained if one measures the experimental hysteresis loop by a local method like the MOKE magnetometer. We are not able to obtain such a local hysteresis loop due

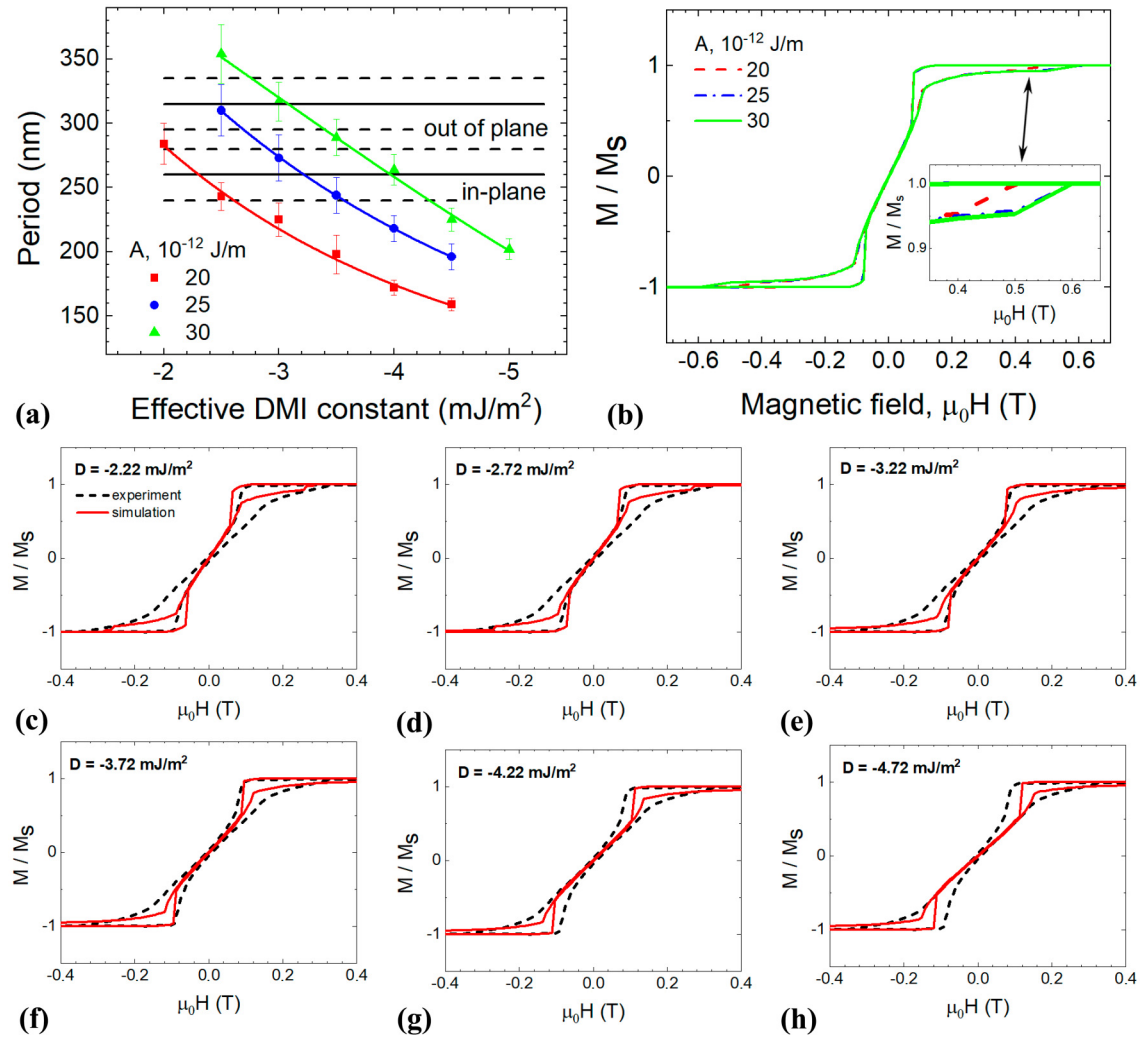

FIG. 6. (a) The dependencies of the periods of simulated magnetic structures of $N20$ superlattices on the energy of effective DMI. (b) Comparison of hysteresis loops of $N20$ samples simulated with parameters $A = 20$, 25, and 30 pJ/m and $D = -2.3$, -3.22, and -4 mJ/m^2, respectively. Hysteresis loops simulated for $N20$ structures with $A = 25$ pJ/m and the values of effective DMI energy: (c) -2.2, (d) -2.72, (e) -3.22, (f) -3.72, (g) -4.22, and (h) -4.72 mJ/m^2.

to the limitation of the out-of-plane magnetic fields available in our station. Second, micromagnetic modeling does not reproduce well the processes of nucleation and annihilation, because of ideal geometry, flat surfaces, and the absence of defects. Various methods are applied to overcome this problem, like including random disturbing magnetic fields and a tilting axis of anisotropy, or including artificial centers of nucleation. Therefore, precise evaluation of DMI energy only by the comparison of experimental and simulated hysteresis loops is difficult. However, comparison of the loops may be useful in testing the results obtained by other approaches, like the modeling of domain periodicity. If the simulated loops completely disagree with the experimental ones, this is a reason for changing the model or simulation parameters.

3. *N5 series and overall results*

$N5$ superlattices are stable in the monodomain state in zero magnetic field; however, they may be demagnetized by an alternate magnetic field with decreasing amplitude. The domain structures of $N5$ samples obtained by the demagnetization procedure in the in-plane and out-of-plane magnetic fields are shown in Figs. 7(a) and 7(b), respectively. The experimentally measured periodicities of the in-plane and out-of-plane demagnetized domain patterns are 600 ± 80 and 780 ± 100 nm. The approach to the determination of the DMI constant used for the $N10$ and $N20$ samples is not applicable in the case of $N5$ films. Artificially created skyrmions in the initial state collapse after relaxation. To simulate the demagnetized state of superlattices which have a ratio $M_r/M_s = 1$ in the hysteresis loop, we tried to use the approach described in [43]. A series of artificially specified rectangular periodic structures with different periodicities were relaxed with given magnetic parameters and a fixed effective DMI constant. The size of the simulation area was 10 μm $\times$ 3 μm $\times$ 14 nm. The cell size was 1 nm $\times$ 1 nm $\times$ 14 nm. The dependence of the total energy density on the domain periodicity $E_{\text{dens.total}}(\lambda)$, was fitted by the function $E_{\text{dens.total}} = E_0 + A\exp(-\frac{\lambda}{t}) + B\lambda$, where E_0, A, B, and t are the fitting parameters. The domain structure with minimal total energy found by differentiation

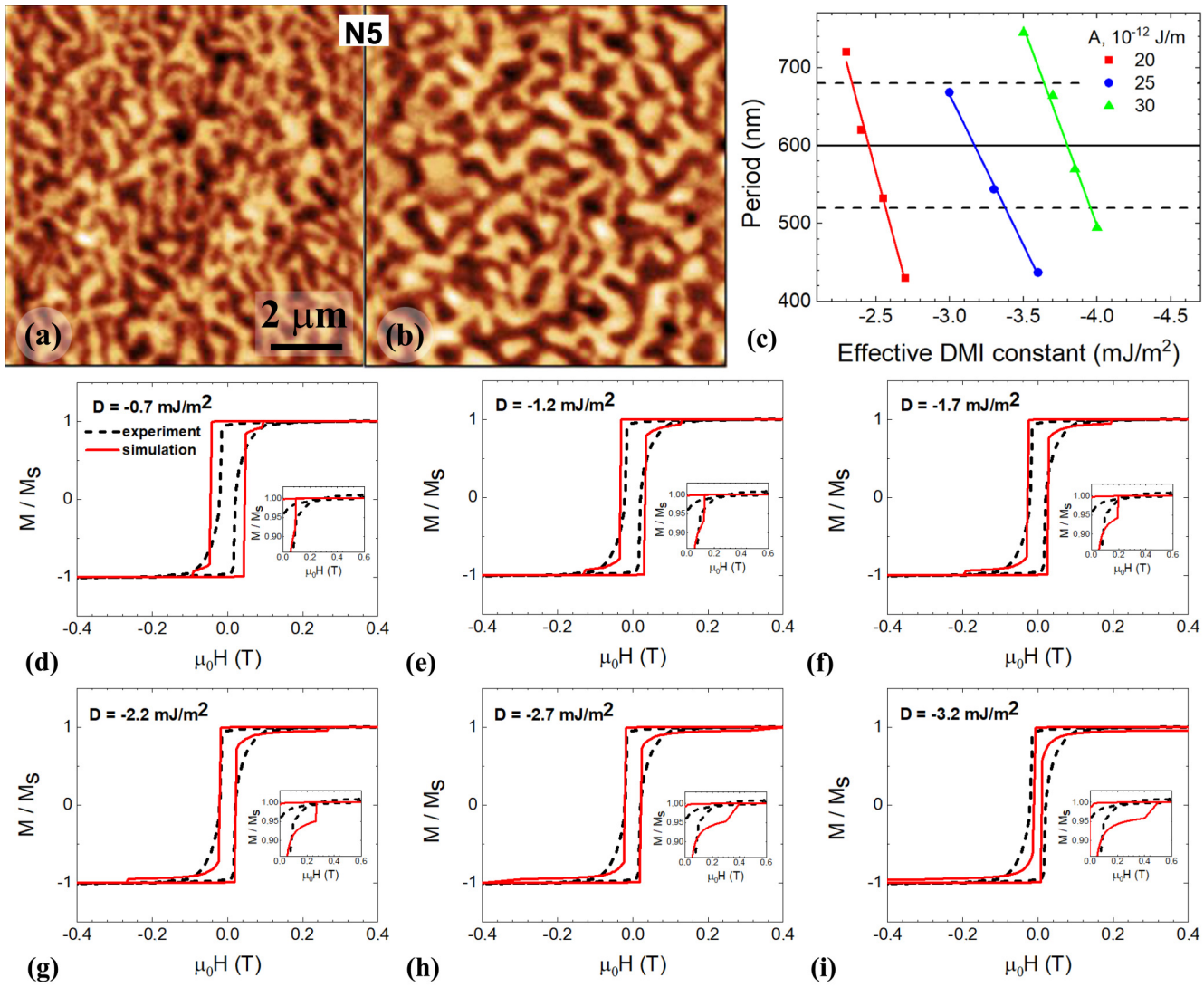

FIG. 7. MFM images of (a) in-plane and (b) out-of-plane demagnetized domain structures of $N5$ superlattices, respectively. (c) Dependencies of periods of simulated domain patterns with minimal total energy density on D_{eff} in $N5$ samples. Experimental and simulated hysteresis loops of $N5$ superlattices with $A = 25\,\text{pJ/m}$ and $D_{\text{eff}} =$ (d) -0.7, (e) -1.2, (f) -1.7, (g) -2.2, (h) -2.7, and (i) $-3.2\,\text{mJ/m}^2$. Annihilation fields of chiral Néel DWs are indicated in the insets.

of the fitted function was considered as the ground state. If the period of the ground simulated structure was not equal to the experimental value, the effective DMI constant was varied until coincidence was achieved. The dependencies of the periodicities of the relaxed domain structures on the effective DMI constants for $A = 20$, 25, and 30 pJ/m are shown in Fig. 7(c). Intersection of the linearly fitted curves with the periodicity of 600 ± 80 nm measured experimentally gives the values of effective DMI energies. The effective DMI constants for the $N5$ superlattices derived by this method with the taken values of exchange constants $A = 20$, 25, and 30 pJ/m are very high: $D = -2.46$, -3.17, and $-3.8\,\text{mJ/m}^2$, respectively.

Therefore, to deduce correct values of the effective DMI energies in $N5$ superlattices we compared the experimentally measured hysteresis loops to the simulated ones. A series of hysteresis loops modeled for $N5$ superlattices with $A = 25\,\text{pJ/m}$ and $|D_{\text{eff}}| = 0.7$, 1.2, 1.7, 2.2, 2.7, and $3.2\,\text{mJ/m}^2$ is shown in Figs. 7(d)–7(i), respectively. The hysteresis loop simulated with $D_{\text{eff}} = -2.2\,\text{mJ/m}^2$ best coincides with the experimental one [Fig. 7(g)]. The simulated loops with lower DMI energies are more rectangular than the experimental one and have lower-annihilation fields of repelling chiral Néel DWs [37], which can be seen in the insets of Figs. 7(d)–7(f). Simulated loops with higher DMI energies are more narrow than the experimental one and have higher-annihilation fields of chiral DWs [Figs. 7(h) and 7(i)]. Since definition of the DMI constant is based only on comparison of hysteresis loops, the error $\pm 0.5\,\text{mJ/m}^2$ for $N5$ superlattices simulated with $A = 25$ pJ is quite large. Based on the approach of comparing the experimental and simulated hysteresis loops, the derived effective DMI energies in $N5$ samples for $A = 20$, 25, and 30 pJ/m are -1.6 ± 0.35, -2.2 ± 0.5, and $-2.7 \pm 0.6\,\text{mJ/m}^2$, respectively (see Table I).

The dependencies of effective DMI energies on the number of Co/Pd bilayers derived with different values of exchange energies used in the calculations are shown in Fig. 8. The first

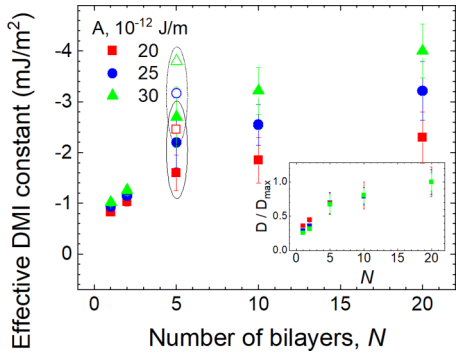

FIG. 8. The dependencies of the effective DMI constants on the period of $[Co/Pd]_N$ superlattices derived for $A = 20, 25$, and 30 pJ/m. Open symbols denote D_{eff} values obtained by relaxation of artificially determined periodic domain structures and comparison of them with experimental ones. The dependencies of effective DMI constants normalized to the $D_{\text{eff}}(N = 20)$ derived for different exchange constants are shown in the inset.

important conclusion is that the magnitude of the effective DMI constant increases with increase of the number of Co/Pd bilayers. Growth of the effective DMI constant is rapid in the beginning and tends to saturation with higher periods of $[Co/Pd]_N$ superlattices. The second conclusion is that the value of exchange energy adopted in the simulations does not influence the trend of the $D_{\text{eff}}(N)$ curve in the range of $N \geqslant 5$. It influences only the quantitative results. The dependencies of the effective DMI constants on the numbers of bilayers normalized to the maximal values of effective DMI energies $D_{\text{eff}}(N = 20)$ in the case of different exchange energies are shown in the inset of Fig. 8. It is seen that all three dependencies practically merge into a single one, except the beginning points at $N = 1$ and 2, which are obtained not by simulation but experimentally. Meanwhile, experimental points obtained by two different methods better correlate with each other if $A = 20$ or 25 pJ/m.

The values of effective DMI energy obtained by comparison of the relaxed, artificially determined periodic domain structures with the experimental ones in the case of the $N5$ samples are indicated by open symbols in Fig. 8. It seems that this approach does not work correctly, at least in the limit of low DMI energies, when the labyrinth domain structure does not spontaneously develop in zero magnetic fields.

D. Discussion

Before discussing the results of this paper, some words need to be said about the existence of DMI in this symmetric system. DMI has been observed in various symmetric systems: Pd/Co multilayers [25] and Pt/Co/Pt trilayers [1,35]. The reasonable explanation of this fact is related to the sensitivity of interfacial DMI to the structure of the interfaces, which may not be equal for the bottom and top interfaces even if the magnetic layer is in contact with the same material. Approval of this proposal may be found in the following papers: Changing the polycrystalline structure of the Pt/Co/Pt trilayers to crystalline structure leads to the DMI vanishing in this system [36]. Changing the stack sequence in Pt/Co/Pd and Pd/Co/Pt trilayers results in different effective DMI energies for these systems [44]. The net DMI in Pt/Co/Pt polycrystalline structures increases as the difference between the top and bottom Co interface quality increases [23]. In this paper we experimentally found at least one reason for the existence of strong DMI in the symmetric system. The bottom Pd/Co and top Co/Pd interfaces are unequally strained in all the layers of the superlattices. This strain asymmetry may cause large DMI in this system. This hypothesis will be experimentally checked in the forthcoming paper. Similar considerations may be found in the works of Pollard *et al.* [25] and Jamali *et al.* [45] to explain nonzero DMI and SOT in symmetric $[Co/Pd]_N$ multilayers, respectively.

It is generally agreed that DMI in multilayer HM1/FM/HM2 structures is of interface origin. This was shown for different systems of materials in various experimental investigations [20] and by *ab initio* calculations [46]. However, from this point of view, the results of the present paper are rather surprising. Since DMI is of interfacial origin, there is no simple explanation for the observed behavior of DMI dependent on the number of Co/Pd bilayers. The increasing number of interfaces is compensated by the increasing volume of Co. Hence, it is reasonable to suppose that the effective DMI energy should remain constant independently of the period of the superlattices. Experimental confirmation of this hypothesis may be found in recent papers concerning multilayers with DMI [24,47]. It is worth noting that in multilayer systems with interface DMI, the effective DMI constant may be expressed as

$$D_{\text{eff}} = \frac{\sum_{i=1}^{N} D_{s,i}/t_{\text{Co}}}{N}, \tag{2}$$

where $D_{s,i}$ is the thickness-independent surface DMI constant of the i-Co layer taking into account the contributions from the bottom and top interfaces and given in J/m, while t_{Co} is the thickness of an individual Co layer.

The effective DMI constant is thickness averaged and given in J/m^2. Increase of the effective DMI constant with increase of the number of bilayers may be obtained if the surface DMI constant depends on the number of chosen bilayers and increases from the bottom to the top Co layers. The roughness of the interfaces increases linearly from the bottom to the top layers of the $[Co/Pd]_N$ superlattices. It may cause the increase of the effective DMI. In the first approximation, it may be supposed that the surface DMI is proportional to the roughness and increases almost linearly from the bottom to the top Co layers. The effective DMI energy of the $N10$ sample is 2.7 times higher than in the $N1$ sample for $A = 25$ pJ/m. If one supposes that D_s of the first layer of the $N10$ superlattice is equal to D_s of the $N1$ sample, then D_s of the tenth Co layer in the $N10$ superlattice must be 4.5 times higher than D_s of the first Co layer, which seems to be rather improbable. It is necessary to conduct a detailed study of the influence of interface roughness on the effective DMI in this system in order to test this hypothesis.

Labyrinth patterns with a given period as in the experiment may be obtained only when the DMI term is taken into account. The hysteresis loops do not coincide with the experimental data without inclusion of DMI in the model. Still, these discrepancies may be explained by incorrect micromagnetic modeling results using the effective layer model. However, precise modeling with all the layers taken into calculation gives similar results. Probably, the micromagnetic modeling does not correctly calculate the demagnetizing energy of such systems, and the decrease of the periodicity of the domains with increase of the number of bilayers is explained only by the balance between the magnetostatic energy and the energy of the DWs. However, results of the micromagnetic modeling coincide well with the analytical calculations in multilayer systems [43]. Nevertheless, we unambiguously detected the chiral structure of the Néel DWs in the $N1$-$N4$ samples, which is the sign of nonzero DMI. Moreover, we are performing a Brillouin-Mandelstam scattering investigation in single-layered Co samples and preliminary results indicate the presence of nonreciprocal propagation of spin waves, which is due to DMI. Results similar to those in the present paper were obtained in polycrystalline Co/Pd multilayers by Pollard *et al.* [25]; they used an experimental technique to evaluate the effective DMI energies. The results of the present work are rather surprising but are based on solid methods and techniques. More experiments in various systems are needed to show whether the dependence of the effective DMI energy on the number of bilayers in multilayered films is inherent only in the Co/Pd system or is more general.

IV. CONCLUSIONS

The structural and magnetic properties of epitaxial Si/Cu/Pd/$[Co/Pd(111)]_N$ superlattices were investigated dependent on the period of superlattices. Co layers are greatly strained in the bottom and less in the top. Asymmetry of the strains is conserved in all Co layers independently of their number. The roughness of the interfaces increases almost linearly from the bottom to the top of the whole structures. PMA does not significantly depend on the period of the superlattices. A strong negative DMI was found in $N1$-$N4$ Co/Pd samples by measuring the asymmetrical velocity of the DWs' propagation in the simultaneous presence of in- and out-of-plane magnetic fields. The effective DMI energy was evaluated in $N5$, $N10$, and $N20$ superlattices by comparison of the experimentally measured out-of-plane hysteresis loops and the in-plane demagnetized domain patterns with results of micromagnetic simulations. An increase of the magnitude of effective DMI energy with increase of the number of Co/Pd bilayers in epitaxial $[Co/Pd(111)]_N$ superlattices was established independently of the value of the exchange constant adopted in the simulations. The method of micromagnetic simulations for DMI evaluation was thoroughly discussed.

ACKNOWLEDGMENTS

The reported study was partially funded by RFBR under the Research Projects No. 18-02-00205 and No. 18-32-20057, and by the Grant program of the Russian President (Grant No. MK-5021.2018.2).

[1] C. Moreau-Luchaire, C. Moutafis, N. Reyren, J. Sampaio, C. A. F. Vaz, N. Van Horne, K. Bouzehouane, K. Garcia, C. Deranlot, P. Warnicke, P. Wohlhüter, J. M. George, M. Weigand, J. Raabe, V. Cros, and A. Fert, Nat. Nanotechnol. **11**, 444 (2016).

[2] O. Boulle, J. Vogel, H. Yang, S. Pizzini, D. De Souza Chaves, A. Locatelli, T. O. Menteş, A. Sala, L. D. Buda-Prejbeanu, O. Klein, M. Belmeguenai, Y. Roussigné, A. Stashkevich, S. Mourad Chérif, L. Aballe, M. Foerster, M. Chshiev, S. Auffret, I. M. Miron, and G. Gaudin, Nat. Nanotechnol. **11**, 449 (2016).

[3] S. Woo, K. Litzius, B. Krüger, M. Y. Im, L. Caretta, K. Richter, M. Mann, A. Krone, R. M. Reeve, M. Weigand, P. Agrawal, I. Lemesh, M. A. Mawass, P. Fischer, M. Kläui, and G. S. D. Beach, Nat. Mater. **15**, 501 (2016).

[4] M. Bode, M. Heide, K. Von Bergmann, P. Ferriani, S. Heinze, G. Bihlmayer, A. Kubetzka, O. Pietzsch, S. Blügel, and R. Wiesendanger, Nature **447**, 190 (2007).

[5] P. Ferriani, K. von Bergmann, E. Y. Vedmedenko, S. Heinze, M. Bode, M. Heide, G. Bihlmayer, S. Blügel, and R. Wiesendanger, Phys. Rev. Lett. **101**, 027201 (2008).

[6] S. Emori, U. Bauer, S. M. Ahn, E. Martinez, and G. S. D. Beach, Nat. Mater. **12**, 611 (2013).

[7] K.-S. Ryu, L. Thomas, S.-H. Yang, and S. Parkin, Nat. Nanotechnol. **8**, 527 (2013).

[8] I. Dzyaloshinsky, J. Phys. Chem. Solids **4**, 241 (1958).

[9] T. Moriya, Phys. Rev. **120**, 91 (1960).

[10] G. Chen, J. Zhu, A. Quesada, J. Li, A. T. N'Diaye, Y. Huo, T. P. Ma, Y. Chen, H. Y. Kwon, C. Won, Z. Q. Qiu, A. K. Schmid, and Y. Z. Wu, Phys. Rev. Lett. **110**, 177204 (2013).

[11] P. Bruno, Phys. Rev. B **39**, 865 (1989).

[12] Yu. A. Bychkov and E. I. Rashba, Pis'ma Zh. Eksp. Teor. Fiz. **39**, 66 (1984) [JETP Lett. **39**, 78 (1984)].

[13] P. P. J. Haazen, E. Murè, J. H. Franken, R. Lavrijsen, H. J. M. Swagten, and B. Koopmans, Nat. Mater. **12**, 299 (2013).

[14] I. M. Miron, T. Moore, H. Szambolics, L. D. Buda-Prejbeanu, S. Auffret, B. Rodmacq, S. Pizzini, J. Vogel, M. Bonfim, A. Schuhl, and G. Gaudin, Nat. Mater. **10**, 419 (2011).

[15] A. Fert, V. Cros, and J. Sampaio, Nat. Nanotechnol. **8**, 152 (2013).

[16] S. Parkin and S. H. Yang, Nat. Nanotechnol. **10**, 195 (2015).

[17] J. Yu, X. Qiu, Y. Wu, J. Yoon, P. Deorani, J. M. Besbas, A. Manchon, and H. Yang, Sci. Rep. **6**, 32629 (2016).

[18] J. Sampaio, V. Cros, S. Rohart, A. Thiaville, and A. Fert, Nat. Nanotechnol. **8**, 839 (2013).

[19] H. J. G. Draaisma, W. J. M. de Jonge, and F. J. A. den Broeder, J. Magn. Magn. Mater. **66**, 351 (1987).

[20] M. Belmeguenai, J. P. Adam, Y. Roussigné, S. Eimer, T. Devolder, J. V. Kim, S. M. Cherif, A. Stashkevich, and A. Thiaville, Phys. Rev. B **91**, 180405 (2015).

[21] A. Samardak, A. Kolesnikov, M. Stebliy, L. Chebotkevich, A. Sadovnikov, S. Nikitov, A. Talapatra, J. Mohanty, and A. Ognev, Appl. Phys. Lett. **112**, 192406 (2018).

[22] A. Belabbes, G. Bihlmayer, S. Blügel, and A. Manchon, Sci. Rep. **6**, 24634 (2016).
[23] A. W. J. Wells, P. M. Shepley, C. H. Marrows, and T. A. Moore, Phys. Rev. B **95**, 054428 (2017).
[24] A. Soumyanarayanan, M. Raju, A. L. G. Oyarce, A. K. C. Tan, M. Y. Im, A. P. Petrovic, P. Ho, K. H. Khoo, M. Tran, C. K. Gan, F. Ernult, and C. Panagopoulos, Nat. Mater. **16**, 898 (2017).
[25] S. D. Pollard, J. A. Garlow, J. Yu, Z. Wang, Y. Zhu, and H. Yang, Nat. Commun. **8**, 14761 (2017).
[26] A. Vansteenkiste, J. Leliaert, M. Dvornik, M. Helsen, F. Garcia-Sanchez, and B. Van Waeyenberge, AIP Adv. **4**, 107133 (2014).
[27] F. J. Lamelas, C. H. Lee, H. He, W. Vavra, and R. Clarke, Phys. Rev. B **40**, 5837 (1989).
[28] M. Wasniowska, N. Janke-Gilman, W. Wulfhekel, M. Przybylski, and J. Kirschner, Surf. Sci. **601**, 3073 (2007).
[29] A. V. Davydenko, A. G. Kozlov, A. V. Ognev, M. E. Stebliy, and L. A. Chebotkevich, Appl. Surf. Sci. **384**, 406 (2016).
[30] A. V. Davydenko, A. G. Kozlov, A. V. Ognev, M. E. Stebliy, A. S. Samardak, K. S. Ermakov, A. G. Kolesnikov, and L. A. Chebotkevich, Phys. Rev. B **95**, 064430 (2017).
[31] C. Kittel, Phys. Rev. **70**, 965 (1946).
[32] C. Kooy and U. Enz, Philips Res. Rep. **15**, 7 (1960).
[33] O. Hellwig, A. Berger, J. B. Kortright, and E. E. Fullerton, J. Magn. Magn. Mater. **319**, 13 (2007).
[34] H. Sakurai, F. Itoh, Y. Okabe, H. Oike, and H. Hashimoto, J. Magn. Magn. Mater. **198**, 662 (1999).
[35] S. G. Je, D. H. Kim, S. C. Yoo, B. C. Min, K. J. Lee, and S. B. Choe, Phys. Rev. B **88**, 214401 (2013).
[36] A. Hrabec, N. A. Porter, A. Wells, M. J. Benitez, G. Burnell, S. McVitie, D. McGrouther, T. A. Moore, and C. H. Marrows, Phys. Rev. B **90**, 020402 (2014).
[37] M. J. Benitez, A. Hrabec, A. P. Mihai, T. A. Moore, G. Burnell, D. Mcgrouther, C. H. Marrows, and S. McVitie, Nat. Commun. **6**, 8957 (2015).
[38] A. Michels, J. Weissmüller, A. Wiedenmann, J. S. Pedersen, and J. G. Barker, Philos. Mag. Lett. **80**, 785 (2000).
[39] H. A. Alperin, O. Steinsvoll, G. Shirane, and R. Nathans, J. Appl. Phys. **37**, 1052 (1966).
[40] X. Liu, M. M. Steiner, R. Sooryakumar, G. A. Prinz, R. F. C. Farrow, and G. Harp, Phys. Rev. B **53**, 12166 (1996).
[41] R. Moreno, R. F. L. Evans, S. Khmelevskyi, M. C. Muñoz, R. W. Chantrell, and O. Chubykalo-Fesenko, Phys. Rev. B **94**, 104433 (2016).
[42] C. Eyrich, A. Zamani, W. Huttema, M. Arora, D. Harrison, F. Rashidi, D. Broun, B. Heinrich, O. Mryasov, M. Ahlberg, O. Karis, P. E. Jönsson, M. From, X. Zhu, and E. Girt, Phys. Rev. B **90**, 235408 (2014).
[43] I. Lemesh, F. Büttner, and G. S. D. Beach, Phys. Rev. B **95**, 174423 (2017).
[44] Y. Guan, T. Koyama, and D. Chiba, AIP Adv. **7**, 085123 (2017).
[45] M. Jamali, K. Narayanapillai, X. Qiu, L. M. Loong, A. Manchon, and H. Yang, Phys. Rev. Lett. **111**, 246602 (2013).
[46] H. Yang, A. Thiaville, S. Rohart, A. Fert, and M. Chshiev, Phys. Rev. Lett. **115**, 267210 (2015).
[47] W. Legrand, J. Chauleau, D. Maccariello, N. Reyren, S. Collin, K. Bouzehouane, N. Jaouen, V. Cros, and A. Fert, Sci. Adv. **4**, eaat0415 (2018).